EE

ISSN 1343-2230
CNS-REP-62
ISSN 1346-244X
RIKEN-AF-NP-458
July, 2004

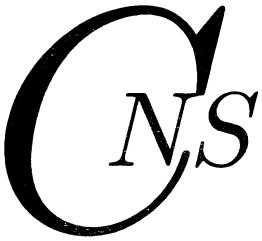

CNS Report

Low-Energy Radioisotope Beam Separator CRIB

Y. Yanagisawa, S. Kubono, T. Teranishi, K. Ue,
S. Michimasa, M. Notani, J.J. He, Y. Ohshiro,
S. Shimoura, S. Watanabe, N. Yamazaki, H. Iwasaki,
S. Kato, T, Kishida, T. Morikawa, and Y. Mizoi

submitted to Nucl. Instr. and Meth. A

Center for Nuclear Study (CNS)

Graduate School of Science, the University of Tokyo
Wako Branch at RIKEN, 2-1 Hirosawa, Saitama 351-0198, Japan
Correspondence: cnsoffice@cns.s.u-tokyo.ac.jp

Low-Energy Radioisotope Beam Separator CRIB

Y. Yanagisawa[a,b,*], S. Kubono[b], T. Teranishi[b], K. Ue[b], S. Michimasa[b], M. Notani[b], J.J. He[b], Y. Ohshiro[b], S. Shimoura[b], S. Watanabe[b], N. Yamazaki[b], H. Iwasaki[b], S. Kato[c], T. Kishida[a], T. Morikawa[d], and Y. Mizoi[a]

[a] *The Institute of Physical and Chemical Research (RIKEN), 2-1, Hirosawa, Wako, Saitama, 351-0198 Japan*

[b] *Center for Nuclear Study (CNS), University of Tokyo, Wako Branch at RIKEN, 2-1, Hirosawa, Wako, Saitama,351-0198 Japan*

[c] *Department of Physics, Yamagata University, Yamagata, 990-8560 Japan*

[d] *Department of Physics, Kyushu University, Hakozaki, Fukuoka, 812-8581 Japan*

Abstract

A low-energy in-flight type RI beam separator, called CRIB, has been installed for nuclear physics and nuclear astrophysics by the Center for Nuclear Study, the University of Tokyo in the RIKEN Accelerator Research Facility. It consists of a double achromatic system and an Wien filter. It is capable of providing RI beams at 5 – 10 MeV/nucleon. Since CRIB has been developed in the end of 2000, many proton-rich RI beams were successfully produced via the (p,n), (d,t), and $(^3He,n)$ reactions in inverse kinematics. In this paper, the design of the separator and its performance are discussed including the method of RI-beam production at low energies.

Key words: In-flight separator, Low energy RI beams
PACS: 29.30.-h, 29.30Aj

* Corresponding author.
Email address: yanagisa@rarfaxp.riken.jp (Y. Yanagisawa).
[1] Present address : Department of Physics, Kyushu University, Hakozaki, Fukuoka, 812-8581 Japan
[2] Present address: The Institute of Physical and Chemical Research (RIKEN), 2-1, Hirosawa, Wako, Saitama, 351-0198 Japan
[3] Present address : Argonne National Laboratory, Argonne, IL 60439 U.S.A.
[4] Present address : Osaka Electro-communication University, 18-8 Hatsu-cho, Nayagawa, Osaka, 572-8530 Japan

Preprint submitted to Nucl. Instr. and Meth. A

1 Introduction

Radioactive isotope (RI) beams at 5 - 10 MeV/nucleon are very useful for nuclear spectroscopy studies, such as particle transfer reactions. Nuclear structure studies with in-beam γ-ray spectroscopy in this energy region, are also powerful, because nuclear fusion reactions have large cross sections. The Center for Nuclear Study (CNS), University of Tokyo has installed a low-energy RI beam separator, called CNS RI-Beam separator (CRIB), in the RIKEN Accelerator Research Facility (RARF) [1]. This separator was developed under the CNS - RIKEN collaboration. The outline of CRIB was described in ref. [2].

Production of RI beams usually is done by two methods: the ISOL-based technique [3] and the in-flight technique [4–7]. The ISOL-based method has an advantage in the beam quality and possibly in the intensity. However, available RI beams are limited because the extraction efficiency in the ion source depends strongly on the element, and also by the life time.

On the other hand, the in-flight method has an advantage in producing the various RI beams,especially of short half-lives. Reaction products are emitted with almost the same velocity as the primary beams in the projectile fragmentation reactions. Therefore, the separation of nuclear species is very simple and has a high collection efficiency. The method has been frequently applied in the energy region of $E \geq 30$ MeV/nucleon, at many facilities such as RIKEN [4], MSU [5], GSI [6] and GANIL [7]. These facilities typically consist of a double achromatic magnetic separator with a degrader. In the fragmentation technique, the isotopic separation is based on momentum analysis of the particles based on their magnetic rigidities before and after the energy changes in the passage through the degrader [8]. The separated isotopes are required to be focused within a small spot size irrespective of their kinetic energies; namely, isotopic separation with achromaticity is required.

The in-flight method at low-energies was not seriously considered before, because the effective production target thickness usable for RI beam production is too thin to produce high intensity beams. However, recent development of ion source technology for heavy ions now enables production of RI beams of reasonably high intensity. Moreover, if one uses two-body reactions such as (p,n) in inverse kinematics, the RI beam emittance can be kept adequately small and comparable to the acceptance of the separator. However, one possible problem for low-energy in-flight separation might come from large energy straggling in the target and degrader for low-energy heavy-ions, which will deteriorate the RI beam quality. This is one of the major concerns here for designing low-energy RI-beam separators.

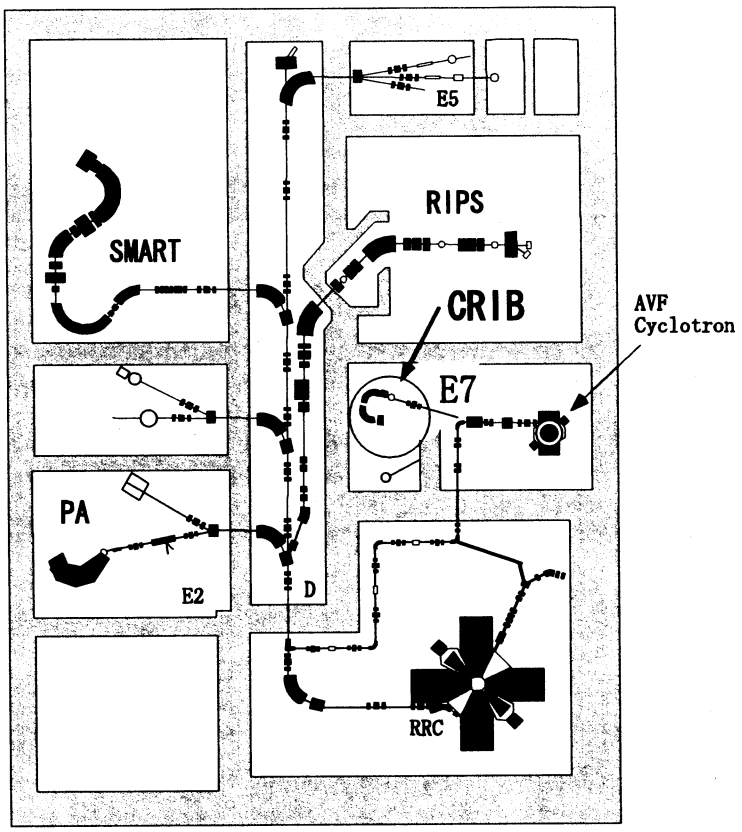

Fig. 1. Layout of the RIKEN Accelerator Research Facility. The CRIB is installed in the E7 room.

To establish an efficient and useful separator facility it is important to optimize the facility components from the ion source to the separator. The accelerator should provide a variety of heavy ion beams with energies up to about 10 MeV/nucleon, with high intensities. Here, we use the AVF cyclotron ($K = 70$) at RARF. Several major developments have been made for the present purpose. Figure 1 shows the layout of the separator CRIB in RARF. The CRIB has been installed in the experimental hall E7. It consists of major parts used before for the spin transfer spectrometer DUMAS [9], at the Research Center for Nuclear Physics (RCNP), Osaka University, and several modifications and new installations have been made. It is comprised of a windowless gas target [10,11] for high beam intensities, a velocity filter (Wien filter) for better RI beam separation, and high-power Faraday cups on the inner dipole walls.

This report describes the design of CRIB and the performance of the double achromatic system. In Section 2, we describe the design characteristics of CRIB, including the beam ion optics and the properties of RI beams. Additionally, the beam diagnostics at each focal plane; Wien filter system, and the windowless gas target are discussed in this section. The performance of CRIB in actual experiments is described in Section 3. A summary is provided in Section 4, including related technological developments and the future outlook of

CRIB.

2 Design of CRIB

The double achromatic part of CRIB, the first half, consists basically of four components: a production target; two dipole magnet systems, and an energy degrader placed in-between. It was designed to provide RI beam of 5 - 10 MeV/nucleon. Its compact design matches the layout of the experimental hall. A degrader, that has a uniform thickness, has been adopted because it is easy to fabricate and the thickness can be accurately controlled. In addition, we have constructed a velocity filter section, the second half, for better isotone separation.

Figure 2 shows the plan view of CRIB. This CRIB is divided into two sections: double achromatic system (Q1-M1-D1-Q2-D2-M2-Q3); and a Wien filter system(Q4-Q5- $\vec{E}\times\vec{B}$ -Q6-Q7)), where Q ,D, M and $\vec{E}\times\vec{B}$ denote quadrupole, dipole, multipole correction magnets, and the velocity separation section, respectively.

2.1 Basic design and the layout of the double achromatic system.

Primary beams from the AVF cyclotron are focused onto the production target (F0). Unstable nuclides produced in-flight at F0 are momentum analyzed in the first section that has the configuration of Q-M-D-Q, and focused dispersively on F1. The primary beam will be stopped in a water-cooled aluminum Faraday cups inside the first dipole magnet, or on a beam stopper at F1. The second section, which has the configuration of D-M-Q, compensates the dispersion of the first section and gives a doubly achromatic focus at F2. The design specifications of the system are summarized in Table 1, and the parameters of the five main magnets are listed in Table 2. The two dipole magnets have a non-constant gap widths in the front halves, which were originally introduced to produce additional multipole magnetic fields as listed in Table 2. These magnets are mounted on a platform which can rotate from -5 deg. to 60 deg. around the center of the F0 scattering chamber. All the magnets have independent power supplies which are controlled by a computer in the counting room. The magnetic fields of the D1 and D2 are monitored by a multiplexed NMR system and a Hall probe system, respectively. Several experiments have already been performed at F2. The Wien Filter section can be connected after the F2, the details of which are described in 2.3.

Table 1
Specifications of CRIB.

Maximum magnetification	1.28 Tm
Momentum range	± 7.5% in momentum
	(±15% in energy)
Maximum solid angle	$\Delta\Omega_{max}$ = 5.6 msr
	(75 mr (H) × 75 mr (V))
Deflection angle	185 deg.
Length of central orbit	L = 7.80 m (ρ=90cm)
1st focal plane (F1)	
Size	40 cm (H) × 8 cm (V)
Horizontal momentum dispersion	1.6 m
Tilted angle	0 deg.
Energy resolution	ΔE/E = 1/350
2nd focal plane (F2)	
Energy dispersion	0
Magnification	M_x = 1.2, M_y = 0.5
3rd focal plane (F3)	
Magnification	M_x = 1.2, M_y = 0.5

Table 2
Main magnets

Dipole	D1	D2		Quadrupole	Q1	Q2	Q3
Pole gap[cm]	60	118		Max. field			
Central ray radius[cm]	900	900		(quadrupole)[kG/cm]	−1.15	0.49	−0.75
Bending angle[deg.]	95	90		(sectupole)[G/cm^2]	81	0.22	0
Max. Field				(octupole)[mG/cm^3]	−0.75	0	0
(dipole)[kG]	14.2	14.2					
(sectupole)[G/cm^2]	−6.3	7.4	(left)				
	0	−2.1	(right)				
(octupole)[mG/cm^3]	0	−130	(left)				
	0	−20.8	(right)				

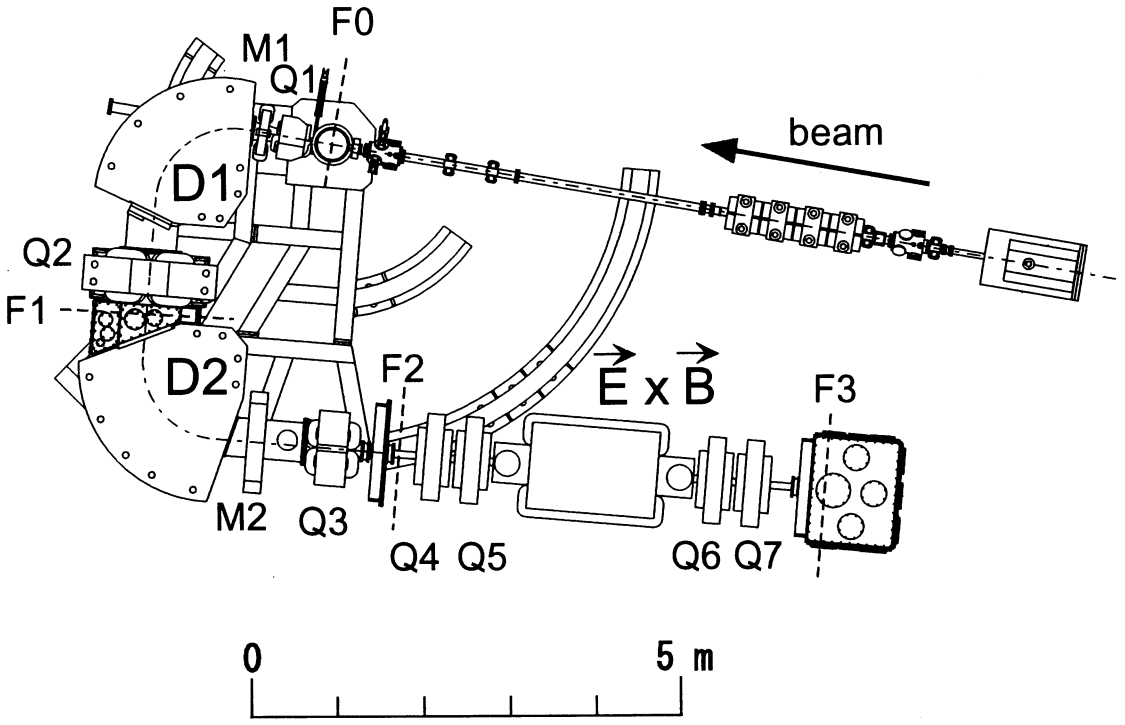

Fig. 2. Plan view of CRIB.

2.2 Ion optics and the characteristics of the double achromatic system

Unstable nuclides produced at the production target are momentum-analyzed in the first half of the system and are then focused dispersively on the degrader, located at F1. The chosen degrader thickness provides an energy loss such that momentum rigidity selection, with the D2 magnet, can be made for the isotope of interest. By design, the momentum dispersion of the first half is canceled out by the D2 magnet, thus, providing an achromatic focusing of particles at F2.

The degrader ion optics matrix elements depend on d/R, where d is the degrader thickness and R is the stopping range of particles in the degrader material. As described by the empirical formula of Dufour et al. [8], it is known that a wedge-shaped degrader may be used to keep the dispersion constant before and after passage through the degrader. In the energy region of a 5 – 10 MeV/nucleon, the thickness of the degrader is typically a few mg/cm^2 to meet the requirement $d/R \leq 0.3$ - 0.6 [12]. However, such a wedge-shaped degrader is too thin to fabricated for our low energy purposes. Therefore, we have instead employed a method that uses a homogeneously thick degrader along with optics tuning that, in combination, is able to realize achromaticity at F2.

Beam optics calculations were performed to determine a degrader matrix el-

ement that would provide achromaticity focusing at F2. Additionally, alternations in the dispersion at F1 can adjust the achromacity at F2 [13]. To achieve this in practice, one can adjust the dispersion at F1 by changing the field strength of the Q2 magnet. For a homogeneous degrader, the dispersion at F1(D_1') can be approximated by $D_1' \sim (1 - d/R)D_1$. Thus, the dispersion should be set to $D_1 = -D_2/M_{x2}/(1 - d/R)$ so that the dispersion after passage through the degrader becomes $D_1' = -D_2/M_{x2}$, satisfying the dispersion compensation relation. Here, D_1, D_2 and M_{x2} denote the energy dispersion from F0 to F1, from F1 to F2, and the magnification factor for x from F1 to F2, respectively.

To simulate the performance of the separator, the profile of the RI beam at the exit of the configuration was calculated by the code GIOS [14]. The third order calculations for the beam envelopes in the horizontal and vertical planes are shown in Fig. 3 by solid lines in the upper and lower parts, respectively. A primary beam emittance of $\Delta\theta_x = \pm$ 30 mrad and $\Delta\theta_y = \pm$ 30 mrad was assumed. The width parameters were set to $\Delta x = \pm 1.5$ mm and $\Delta y = \pm 1.5$ mm for the primary beam at the production target in the horizontal and vertical planes, respectively. The degrader was assumed to be made of aluminum of 12 μm thickness ($d/R = 0.1$).

As shown in the figure, only horizontal focusing is achieved at F1, while at F2 the beam is doubly focused. The magnification from F0 to F1 is 0.3 for x, and those from F0 to F2 are 1.2 for x and 0.5 for y. The momentum dispersion in the horizontal direction is also shown by the dashed line in Fig. 3. It is seen that the dispersion at F1 is determined by the magnetic fields of the D1 and Q2 magnets. The horizontal width of the beam envelope at the F1 focal plane defines the momentum acceptance and the maximum setting available is about $\pm$7.7%. Depending on experimental requirements, the beams can be focused within a range of about 1m from F2, which can be accomplished by adjusting of the Q3 or M2 magnets.

2.3 Wien filter

The Wien filter system is attached to the downstream side of F2 to provide additional background suppression of undesired isotopes. The filter can provide a pure RI beam without deteriorating the beam size. One may use the Wien filter without the degrader, where the RI beam size can be much smaller than in the case with a degrader, because the straggling at the degrader mainly determines the RI beam sizes. Furthermore, it can be used to measure fusion products of reactions with RI beams at F2. Note that complete fusion products cannot be separated with any magnetic separators, because their momenta do not change by the reaction. Of course, the filter is useful

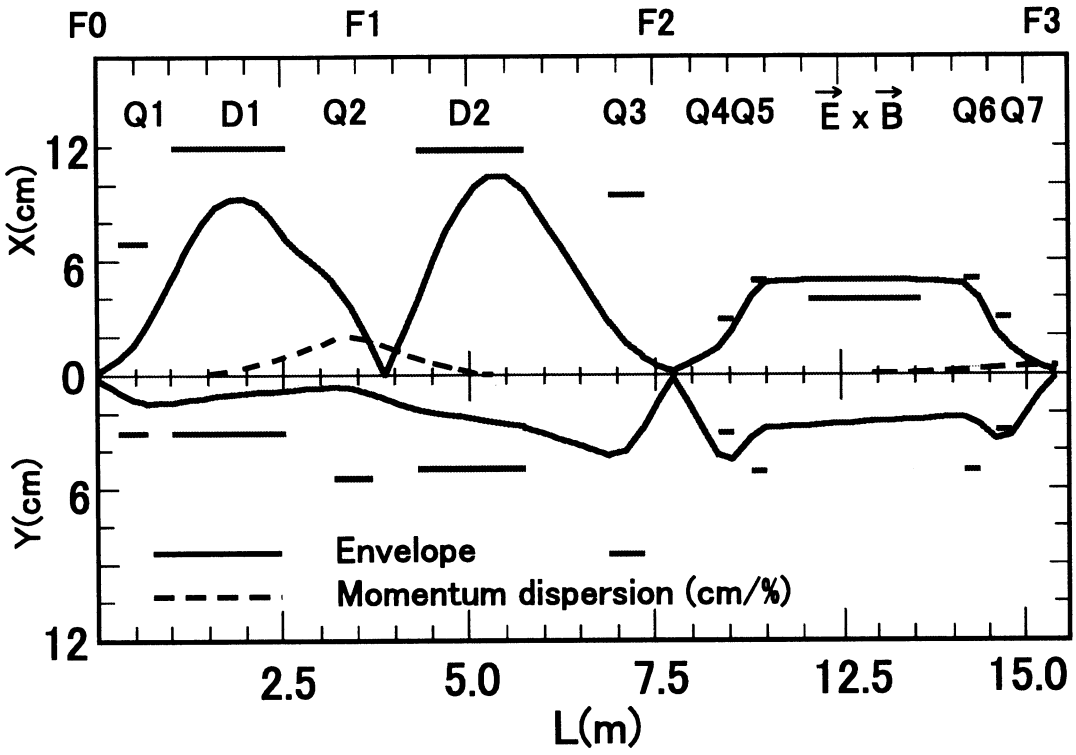

Fig. 3. Ion optical calculation of the combined CRIB - Wien Filter system for the 6.94 MeV/nucleon ^{14}O beam by using the code GIOS.

when the energy-degrader method is insufficient, for example, in separating a proton-rich nuclide from the neighboring isotones.

The Wien filter system is 5-m long. It consists of four quadrupole magnets (Q4, Q5, Q6 and Q7) and a velocity separation section (1.5 m long) between Q5 and Q6. The magnification from the entrance (F2) to the exit (F3) is 1.0 for a typical operation. The maximum field gradients are 0.97 kG/cm for Q4 and Q7, and 1.8 kG/cm for Q5 and Q6. Their gradients are large enough to transport particles with the maximum magnetic rigidity of the CRIB line. The velocity separation section ($\vec{E} \times \vec{B}$) consists of a dipole magnet with a 45-cm pole gap and two electrodes mounted in the gap space. The electrodes are set in parallel along the beam axis separated by an 8-cm gap. High voltages ($\pm$200 kV at maximum) are applied to the electrodes to make a horizontal electric field (50 kV/cm at maximum), which is combined with the vertical magnetic field (2.9 kG maximum) to provide $\vec{E} \times \vec{B}$ filtering.

As an example, Fig. 3 displays a third-order calculation by the code GIOS [14] for CRIB optics, including the Wien Filter, for a 6.94-MeV/nucleon ^{14}O beam. The $\vec{E} \times \vec{B}$ field produces a velocity dispersion in the horizontal direction. The maximum dispersion is expected to be 0.6 cm/% for ^{14}O with settings of E = 49 kV/cm and B = 1.35 kG. The velocity resolving power $v/\Delta v$ is about 100 if the horizontal beam spot size is 1.0 cm at F2. The transport efficiency

from F2 to F3 is 40% in this condition. All the elements of the Wien filter are mounted on a movable frame which can be detached from the main chassis of CRIB. When the Wien filter is not in use, its frame can be moved aside to a parking position to make a larger experimental space around F2.

2.4 Windowless gas target

Because the energy range of primary beams is 5 - 10 MeV/nucleon, the production target thickness should be around 1 mg/cm^2, or less. In several experiments at CRIB, solid targets, or gas targets confined in a cell with windows, were used. However, such thin solid target materials, as well as the windows, can easily be deteriorated by heat caused by the primary beams as their beam intensities become high. A windowless gas target system is suitable to solve this heat problem. It is also useful to avoid background particle production from reactions in the window foils.

The windowless gas target system developed for CRIB have the same structure as that in ref. [10], but with an extensive gas recirculation system. It consists of a differential pumping system and a blow-in type gas cell, which was developed by Sagara *et al.* [11]. A target thickness of about 1 mg/cm^2 was obtained for nitrogen gas. The gas recirculation system may reduce gas consumption and also solve the serious problem reported in ref. [15]. The oil from the vacuum pumps was also recirculated into the target cell, and the carbon in the oil was precipitated like agrestal field on the inside wall of the target cell after long irradiation by intense beams. The system, therefore, has adopted a purification section in the recirculation line, which includes a cold trap system cooled with solid carbon dioxide. This purification section works very well, and all other problems reported in ref. [15] have been also overcome in the present gas target system. The system also has other capabilities such as a high sensitive monitor of oxygen to avoid explosive hydrogen buring in case of hydrogen gas target.

2.5 Beam monitors

A beam diagnostic device is situated at each focal plane. The profile of primary beam can be monitored with a ZnS beam viewer at F0, and with a single-wire profile monitor at 65 cm upstream of F0. The RI beam profile is measured at each focal plane using parallel plate avalanche counters (PPAC) with segmented horizontal and vertical cathodes [16]. The PPAC at F1 is used for the momentum measurement, and the one at F2 can be used for observing the isotopic separation and for tuning RI-beam profile at the secondary target position. By using two PPACs, each beam particle can be tracked to identify the incident angles and the reaction point.

Table 3
Beam diagnosis devices.

Location	Device
F0	Single-wire profile monitor for primary beam
	Beam viewer (ZnS) on a target folder
	Faraday cup
	Aperture for defining acceptance angle (F0 slit)
F1	Aperture for defining momentum acceptance
	PPAC for position and timing measurements
	Energy degrader for separating beams
F2	Aperture for isotope separation
	PPAC for position and timing measurements
	Silicon detector for energy measurement
F3	Aperture for isotope separation
	PPAC for position and TOF measurements
	Silicon detector for energy measurement
D1	NMR probe
D2	Hall probe
Inside of D1	Primary-beam stopper(water cooled)

Particle identification of RI beams is performed at F2 by a combination of $B\rho$, time-of-flight (TOF), and energy-loss(E) information after momentum analysis. The TOF is measured between RF signals from the AVF cyclotron and the timing signal from the PPAC. The E is measured by a silicon detector placed at F2. By looking at the particle identification spectrum and the beam profile, the magnetic rigidity of D2 and the focusing condition of Q magnets can be adjusted so as to select an isotope of interest. The properties of these diagnostic devices are summarized in Table 3.

3 Experimental study of the performance at F2

To establish an efficient method of producing low-energy RI-beams, we performed a test experiment to produce an ^{14}O beam at 6.9 MeV/nucleon. A primary beam of $^{14}N^{6+}$ at 8.4 MeV/nucleon bombarded a gas target of 1.5 mg/cm^2 CH_4. The production target was confined in a small gas cell with the

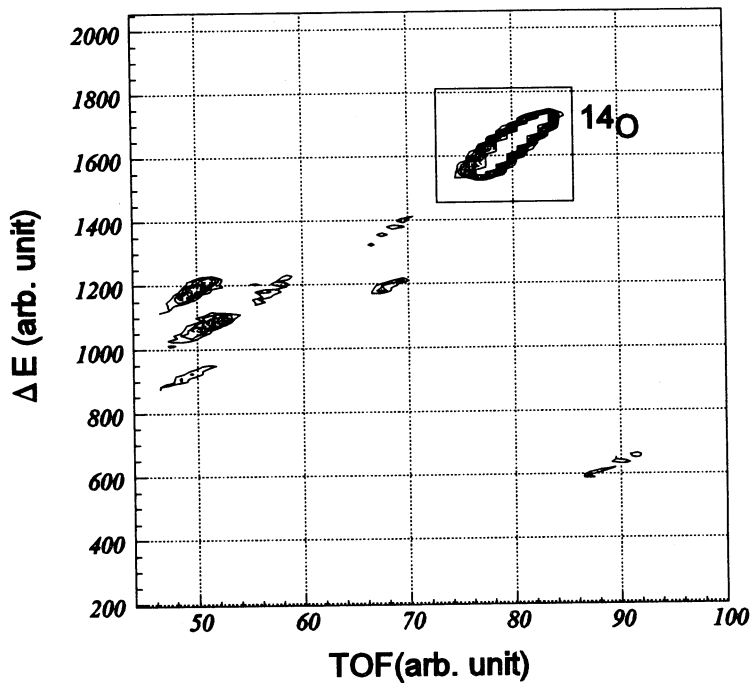

Fig. 4. Two-dimensional plot of TOF versus energy loss, obtained by ^{14}N beam on a CH_4 target.The ^{14}O beam was clearly separated from contaminants.

entrance and exit windows made of 2.2 μm-thick Havar foils. An ^{14}O beam produced by the ^{14}N (p,n) ^{14}O reaction in inverse kinematics was transported to F1. We installed an aluminized-mylar foil with a thickness of 1.7 mg/cm^2, which corresponds to $d/R = 0.1$, as a homogeneous degrader at F1. The momentum acceptance was set to 5% by a variable aperture at F1. The ^{14}O beam, having passed through the degrader, was transported to F2. There, the ^{14}O beam particles were identified by TOF, measured between the RF and the PPAC, combined with the energy loss of particles in the silicon detector, as shown in Fig. 4. In this spectrum, the ^{14}O beam was clearly separated from contaminants. The beam purity of ^{14}O at F2 was approximately 85%, with the main background being ^{14}N scattered from the wall of D1, the beam pipe and the target cell. The ^{14}O beam intensity was 1.0×10^6 cps for the ^{14}N primary beam of 500 pnA.

We also performed a measurement to verify the achromaticity. Experimentally, the horizontal centroid position of the ^{14}O beam profile was measured at F2 as a function of momentum under three conditions; (1) without degrader, (2) with degrader and re-tuning the magnets, and (3) with degrader but without re-tuning the magnets. The momentum spread was set to 0.13% using the momentum aperture and the aperture position was scanned from 0 to 50 mm from the central orbit at F1. Note that the spot size of ^{14}N primary beam at F2 is 1.2 mm ($\Delta x_{^{14}\mathrm{N}}$) $\times$ 1.0 mm ($\Delta y_{^{14}\mathrm{N}}$) in σ.

Figure 5 shows the centroid position, x_2, at F2, as a function of aperture

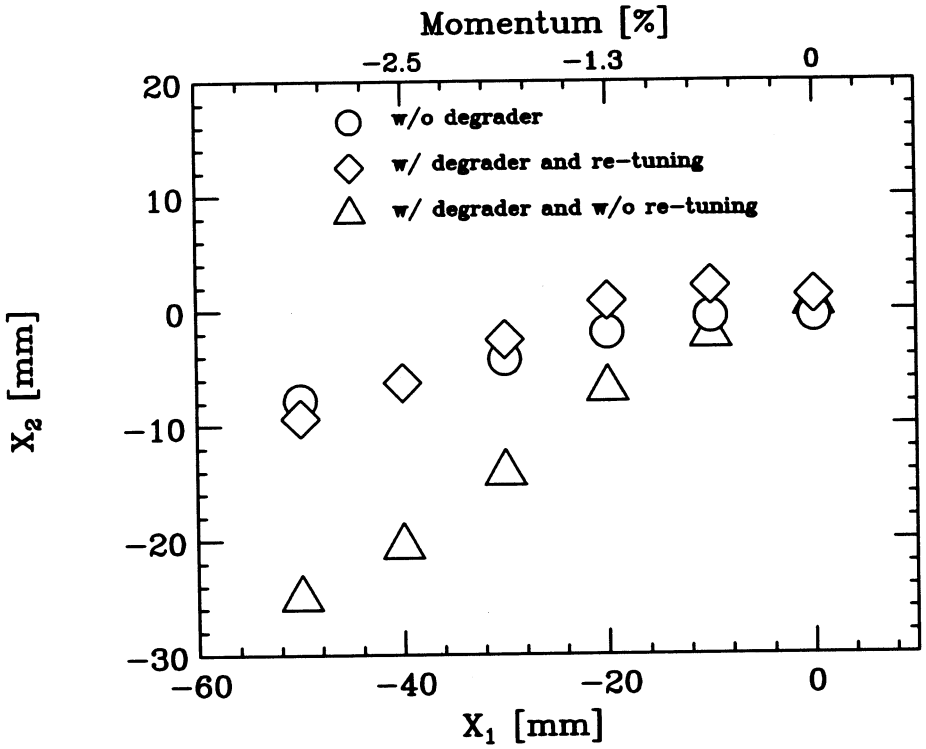

Fig. 5. The horizontal centroid position of the ^{14}O beam at F2 as a function of its momentum, measured with an aperture of 0.13%. The positions x_1 = 0, −10, −20, −30, −40, and −50 mm correspond to 0, −0.63, −1.3, −1.9, −2.5, and −3.2% respectively, in deviation from the central momentum. The momentum is the difference from the central orbit.

position, x_1, at F1, which defines the momentum of ^{14}O. When the degrader was not used, the shift at x_2 was measured to be 8 mm at $x_1 = -50$ mm. In the case where the degrader was used and the optics were re-adjusted, the shift was 9 mm at $x_1 = -50$ mm. Both values of the shift were significantly smaller than $x_2 = 25$ mm at $x_1 = -50$ mm obtained with the degrader and no re-adjustment. This indicates that the re-adjustment of the separator system is definitely required for the use of homogeneously-thick degrader. The spot size of ^{14}O at F2, shown by the triangular symbols, is approximately 10.5 mm (Δx_{deg}) × 3.5 mm (Δy_{deg}) in σ.

There are two main contributions for the large spot size. One is an aberration of the optics, present when the multiple elements are not applied. The effect of the aberration was estimated from the run with a low intensity primary beam and the run for ^{14}O production without the degrader. The results yield a spread of the ^{14}O RI-beam estimated to be 7.6 mm in $\Delta x_{w/o-deg}$ and 2.8 mm in $\Delta y_{w/o-deg}$. The spread of spot size for aberration are 7.4 mm ($\sigma_x(abe)$) and 2.7 mm ($\sigma_y(abe)$) from $\Delta x_{w/o-deg} = \sqrt{(\Delta x_{^{14}\mathrm{N}})^2 + (\sigma_x(abe))^2}$ and $\Delta y_{w/o-deg} = \sqrt{(\Delta y_{^{14}\mathrm{N}})^2 + (\sigma_y(abe))^2}$, respectively.

Table 4
Intensities of radioactive beams.

RI beam	^{10}C	^{11}C	^{12}N	^{14}O
Intensity (cps)	1.6× 10^5	1.6× 10^4	2.5 × 10^3	1.0 × 10^6
Energy (per nucleon)	6 MeV	3 MeV	4 MeV	7 MeV
Primary beam	$^{10}B^{4+}$	$^{10}B^{4+}$	$^{10}B^{4+}$	$^{14}N^{6+}$
Energy(per nucleon)	7.8 MeV	3.4 MeV	7.8 MeV	8.4 MeV
Reaction	(p,n)	(^{3}He,pn)	(^{3}He,n)	(p,n)
Target	CH_4	^{3}He	^{3}He	CH_4
	1.3 mg/cm^2	0.25 mg/cm^2	0.25 mg/cm^2	1.3 mg/cm^2
Intensity (pnA)	200	200	200	500

The other contribution for the large spot size comes from the large energy loss straggling in the degrader. This influence was estimated from measurements with, and without, the degrader to be 7.2 mm in $\sigma_x(str)$ and 2.0 mm in $\sigma_y(str)$ from $\sqrt{(\Delta x_{deg})^2 - (\Delta x_{w/o-deg})^2}$ and $\sqrt{(\Delta y_{deg})^2 - (\Delta y_{w/o-deg})^2}$, respectively. The estimated $\sigma_x(abe)$ and $\sigma_y(abe)$ from the measurement was consistent with the optical calculation result of 5.7 mm ($\sigma_{xcal}(abe)$) and 1.6 mm ($\sigma_{ycal}(abe)$), respectively.

These result means that the large spot size at F2 comes from the same extent of influence of the aberration of the optics and the energy loss straggling. If the multipole elements are used, the aberration contribution might be significantly reduced. This will be examined in the near future. As shown in Fig. 4, CRIB works reasonably well with the degrader of $d/R = 0.1$. However a thicker degrader, such as with $d/R = 0.3$ often used at higher energies, may not work due to the energy loss straggling.

Experiments for RI beam production with the $^{10}B(^3He, n)$ reaction were also performed. A $^{10}B^{4+}$ beam of 7.8 MeV/ nucleon, with a typical intensity of 200 pnA, bombarded the gas target of ^{3}He with a thickness of 0.25 mg/cm^2. A mylar foil of 10 μm ($d/R = 0.1$) was used for the homogeneous degrader. Produced RI beams were identified by the TOF between the RF signal from the cyclotron and a timing signal of the PPAC. A ^{12}N beam was obtained via the (^3He,n) reaction together with ^{10}C, ^{11}C, and ^{10}B. The RI beam intensities of ^{12}N and ^{11}C were about 2.5 × 10^3 cps and 1.6 × 10^4 cps, respectively. By using these RI beams, resonance-search experiments for the systems ^{11}C + p and ^{12}N + p were performed [17]. Some RI beams obtained by CRIB are summarized in Table 4.

4 Summary

A low-energy RI beam separator of the in-flight type CRIB has been developed. It uses charge exchange reactions as well as particle-transfer reactions in inverse kinematics for RI-production. The separator has two-dipole magnets and a homogeneously-thick energy degrader in-between. The spot size of an RI beam was dominated by energy loss straggling in the degrader and the abberation of the optics. The proper thickness of the degrader was limited by the effects of the energy loss straggling. A value of 0.1 is a practical d/R in the present energy region. The present experimental results with the CRIB facility demonstrate that RI beam production using the in-flight technique is very useful even at 5 - 10 MeV/nucleon. The success of CRIB suggests that low-energy RI beam facilities can be built even at small accelerator facilities.

During the installation of CRIB, we also renewed the beam line from the AVF cyclotron for better transport efficiency, and installed a 14-GHz ECR ion source, called Hyper ECR [20]. The primary beam intensity has been increased by one to two orders of magnitude at F0, resulting in more intense RI-beams production. Currently, we have obtained an RI-beam intensity of about 1×10^6 from (p,n) reactions. This number will be further increased in near future by improving the performance of the ion source and the acceleration efficiency of the AVF cyclotron, as well as target technology. They included a successful introduction of a flat-top accelerator mode for the AVF cyclotron, for instance. Therefore, CRIB has a good prospect for experimental studies both in nuclear physics and nuclear astrophysics, as well as for other applications.

Current experimental programs at CRIB include: (1) resonant elastic scattering experiments for the nuclear structure and nuclear astrophysics study, (2) measurements of reaction cross sections of astrophysical interest, and (3) γ-ray spectroscopy via fusion reactions. Several experiments at CRIB already have been performed successfully by using ^{11}C, ^{12}B, ^{21}Na, and ^{22,23}Mg beams [17–19].

For nuclear astrophysics, higher-quality and higher-purity RI beams are required. The Wien filter and the windowless gas target system have been developed [10,11]. These are essential for high intensity RI-beams with high purity. RI beams of heavier nuclides at about $A = 50$ -60 will be produced in fusion evaporation reactions with the windowless gas-target system.

We expect that longer time can be devoted to the use of CRIB after the RI-Beam Factory at RIKEN starts to operate because the AVF cyclotron, the primary beam source of CRIB, will be no longer used as an injector for the major cyclotron.

Acknowledgements

Sincere gratitude is extended to the staff members of the RIKEN Ring Cyclotron for their help during the installation of CRIB and for their operation of the ECR ion source and the accelerator during the experiment. The authors gratefully owe M. Ishihara, H. Sakai, Y. Yano, and M. Kase for their support and encouragement during this work. We are indebted to T. Noro at Kyushu University and T. Kubo at RIKEN for valuable discussion. We are also grateful to C.C. Yun, S. Bishop and T. Motobayashi for the comments. One of the authors (Y.Y) is grateful for the Special Postdoctoral Researcher Program in RIKEN. This work is partially supported by Grant-in-Aid for Science Research from the Japan Ministry of Education, Culture, Sports, and Technology under contract number 13440071 and 14740156.

References

[1] Y. Yano, *Proc. of 12th Int. Conf. on Cyclotrons and their Applications*, Berlin, eds. B. Martin, and Z. Ziegler (World Scientific, 1989) p. 13.

[2] S. Kubono, Y. Yanagisawa, T. Teranishi, S. Kato, T. Kishida, S. Michimasa, Y. Ohshiro, S. Shimoura, K. Ue, S. Watanabe, and N. Yamazaki, Eur. Phys. J **A13** (2002) 217.

[3] For example, D. Darquennes, P. Decrock, Th. Delbar, W. Galster, M. Huyse, Y. Jongen, M. Lacroix, O, Leleux, I. Licot, E. Liénard, M. Liselet, G. Ryckewaert, Sindano Wa Kitwanga, P.Van Duppen, J. Vanhorenbeeck, J. Vervier, and S. Zaremba, Phys. Rev. C **42** (1990) R804.; L. Buchmann, J.M. D'Auria, J.D. King, G. Mackenzie, H. Schneider, R.B. Moore, and C. Rolfs, Nucl. Instr. Meth. **B26** (1987) 151.

[4] T. Kubo, M. Ishihara, N. Inabe, H. Kumagai, I. Tanihata, K. Yoshida, T. Nakamura, H. Okuno, S. Shimoura, and K. Asahi, Nucl. Instr. Meth. **B70** (1992) 309.

[5] B.M. Sherrill, D.J. Morrissey, J.A. Nolen Jr., and J.A. Winger, Nucl. Instr. Meth. **B56/57** (1991) 1106.

[6] H. Geissel, P. Armbruster, K.H. Behr, A. Brunle, K. Bürkard, M. Chen, H. Folger, B. Folger, B. Franczak, H. Keller, O. Klepper, B. Langenbeck, F. Nickel, E. Pfeng, M. Pfützner, E. Roeckl, K. Rykaczewski, I. Schall, D. Schardt, C. Scheidenberger, K.-H. Schmidt, A. Schröter, T. Schwab, K. Sümmerer, M. Weber, G. Münzenberg, T. Brohm, H.-G. Clerc, M. Fauerbach, J.-J. Gaimard, A. Grewe, E. Hanelt, B. Knödler, M. Steiner, B. Voss, J. Weckenmann, C. Ziegler, A. Magel, H. Wollnik, J.P. Dufour, Y. Fujita, D.J. Vieira, and B. Sherrill, Nucl. Instr. Meth. **B70** (1992) 286.

[7] A.C. Mueller, and R. Anne, Nucl. Instr. Meth. **B56/57** (1991) 559.

[8] J. P. Dufour, R.Del Moral, H. Emmermann, F. Hubert, D. Jean, C. Poinot, M.S. Pravikoff, A. Fleury, H. Delagrange, and K.-H, Schmidt, Nucl. Instr. Meth. **A248** (1986) 267.

[9] T. Noro, T. Takayama, H. Ikegami, M. Nakamura, H. Sakaguchim H. Sakamoto, H. Ogawa, M. Yosoi, T. Ichihara, N. Isshiki, M. Ieri, Y. Takeuchi, H. Togaya, T. Tsutsumi, and S. Kobayashi, J. Phys. Soc. Jpn. **55** (1986) 470.

[10] T. Kishida, Y. Gono, M. Shibata, H. Watanabe, T. Tatsumi, S. Motomura, E. Ideguchi, X.H. Zhou, T. Morikawa, T. Kubo, and M. Ishihara Nucl. Instr. Meth. **A438** (1999) 70.

[11] K. Sagara, A. Motoshima, T. Fujita, H. Akiyoshi, and N. Nishimori, Nucl. Instr. Meth. **A378** (1996) 392.

[12] T. Shimoda, H. Miyatake and S.Morinobu, Nucl. Instr. Meth. **B70** (1992) 320

[13] S. Mitsuoka, T. Shimoda, H. Miyatake, Y. Mizoi, H. Kobayashi, M Sasaki, T. Shirakura, N. Takahashi, T. Murakami, and S. Morinobu, Nucl. Instr. Meth. **A372** (1996) 489.

[14] H. Wollnik, *Optics of Charged Particles*, Academic Press, Orlando, 1987.

[15] T. Kishida, H. Watanabe, E. Ideguchi, T. Kubo, Y.F. Yang, M. Ishihara, S. Yamamoto, Y. Gono, T. Morikawa, T. Tsunami, T. Fukuchi, S. Motomura, H. Tsuchida, O. Kashiyama, K. Saitoh, M. Shibata, A. Odahara, Y.H. Zhang, X.H. Zhou, B. Cederwall, T. Back, and D. Bucurescu, Nucl. Instr. Meth. **A484** (2002) 45.

[16] H. Kumagai, A. Ozawa, N. Fukuda, K. Sümmerer, and I. Tanihata, Nucl. Instr. Meth. **A470** (2001) 562.

[17] T. Teranishi, S. Kubono, S. Shimoura, M. Notani, Y. Yanagisawa, S. Michimasa, K. Ue, H. Iwasaki, M. Kurokawa, S. Satou, T. Morikawa, A. Saito, H. Baba, J.H. Lee, C.S. Lee, Zs. Fülop, and S. Kato, Phys. Lett. **B556** (2003) 27. ; T. Teranishi, S. Kubono, S. Shimoura, M. Notani, Y. Yanagisawa, S. Michimasa, K. Ue, H. Iwasaki, M. Kurokawa, S. Satou, T. Morikawa, A. Saito, H. Baba, J.H. Lee, C.S. Lee, Zs. Fülop, and S. Kato, Nucl. Phys. **A718** (2003) 207c.

[18] J.J. He, S. Kubono, T. Teranishi, M. Notani, H, Baba, S. Nishimura, J.Y. Moon, M. Nishimura, S. Michimasa, H. Iwasaki, Y. Yanagisawa, N. Hokoiwa, M. Kibe, J.H. Lee, S. Kato, Y. Gono, and C.S. Lee, *Proc. of Origin of Matter and Evolution of Galaxies 2003*, World scientific, in press.

[19] T. Teranishi, S. Kubono, J.J. He, M. Notani, T. Fukuchi, S. Nishimura, M. Nishimura, Y. Wakabayashi, N. Hokoiwa, Y. Gono, A. Odahara, H. Ishiyama, Y.X. Watanabe, T. Hashimoto, T. Ishikawa, Y.H. Tanaka, H. Miyatake, J.Y. Moon, J.H. Lee, J.C. Kim, C.S. Lee, V. Guimarães, R.F. Lihitenthaler, H. Baba, K. Sato, T. Kawamura, and S. Kato, *Proc. of Origin of Matter and Evolution of Galaxies 2003*, World scientific, in press.

[20] Y. Ohshiro, S. Watanabe, Y. Higurashi, T. Kageyama, M. Kidera, T. Nakagawa, M. Kase, S. Kubono, and T. Katayama, RIKEN Accel. Prog. Rep. **36** (2003) 279.